UDC 691.537
IRSTI 67.09.33
RESEARCH ARTICLE

STRESS ANALYSIS OF CEMENT CONCRETE PAVEMENTS UNDER TRAFFIC LOADS

L.T. Kabdyrova[1,*], R.E. Lukpanov[1], F.B. Abdushkurov[2], M. Karacasu[3]

[1]L.N. Gumilyov Eurasian National University, 010000, Astana, Kazakhstan
[2] Technobius, LLP, 010000, Astana, Kazakhstan
[3]Eskisehir Technical University, 26000, Eskisehir, Turkey

Abstract. *The paper presents calculations of load-induced normal stresses generated by various vehicle types for subsequent modeling of the abrasion resistance of impregnating compositions in cement concrete pavements. The aim of the study was to evaluate normal stresses arising from vehicular loading, taking into account variations in the tire-pavement contact area due to changes in tire pressure. The study evaluates normal stress levels under vehicular loading, accounting for variations in the tire-pavement contact area associated with changes in tire pressure. Vehicles ranging from bicycles to heavy trucks were classified into categories A1-A5 in ascending order of weight. The results are expressed as ranges, where lower bounds correspond to the lightest vehicles within each category at minimum tire pressure, and upper bounds correspond to the heaviest vehicles at maximum tire pressure. Tire pressure is shown to significantly affect the pavement stress state, increasing normal stresses by 28.6-30.3% (bicycles); 30.9-33.5% (motorcycles); 31.8-32.9% (passenger cars); 31.9-33.2% (light commercial vehicles); 31.9-33.3% (heavy vehicles). The presented calculations are of interest for modeling design scenarios in both experimental studies and numerical simulations. The obtained calculation results will enable more accurate development of design schemes in numerical or large-scale modeling of road scenarios.*

Keywords: *cement concrete pavement, contact stress, tire pressure, traffic loads, pavement loading simulation, numerical modeling*

***Corresponding author**
Lyailya Kabdyrova, e-mail: leila_0781@mail.ru

https://doi.org/10.51488/1680-080X/2026.1-14
Received 04 February 2026; Revised 18 February 2026; Accepted 05 March 2026

ӘОЖ 691.537
ҒТАМР 67.09.33
ҒЫЛЫМИ МАҚАЛА

КӨЛІК ЖҮКТЕМЕЛЕРІ ӘСЕРІНЕН ЦЕМЕНТБЕТОН ЖАБЫНДАРЫНДАҒЫ КЕРНЕУЛЕРДІ ТАЛДАУ

Л.Т. Кабдырова[1,*], Р.Е. Лукпанов[1], Ф.Б. Абдушкуров[2], М. Караджасу[3]

[1]Л.Н.Гумилев атындағы Еуразия ұлттық университеті, 010000, Астана, Қазақстан
[2]«Технобиус» ЖШҚ, 010000, Астана, Қазақстан
[3]Эскишехир техникалық университеті, 26000, Эскишехир, Түркия

Аңдатпа. *Мақалада цементбетон жол жабындарындағы сіңіргіш қоспалардың тозуға төзімділігін модельдеуге арналған әртүрлі көлік құралдарының әсерінен туындайтын нормаль кернеулердің есептеулері берілген. Зерттеудің мақсаты - көлік құралдарының әсерінен туындайтын нормаль кернеулерді шинаның қысымын төмендету немесе көтеру нәтижесінде өзгеретін контактілік алаңды ескере отырып бағалау болды. Жұмыста шинаның жол бетімен контактілік ауданының өзгермелілігін есепке ала отырып, транспорттық жүктемелердің әсерінен нормаль кернеу деңгейлері бағаланды. Велосипедтерден бастап ауыр жүк көліктеріне дейінгі көлік құралдары массасына қарай өсу тәртібімен А1-А5 категорияларына бөлінді. Нәтижелер диапазон түрінде берілген, мұнда төменгі шектер әр категориядағы ең жеңіл көлік құралдарына минималды шиналық қысым кезінде, ал жоғарғы шектер ең ауыр көліктерге максималды шиналық қысым кезінде сәйкес келеді. Шиналық қысым жол жабындарының кернеу жағдайына айтарлықтай әсер ететіндігі көрсетілді, нормаль кернеулердің артуы: 28.6-30.3% (велосипедтер); 30.9-33.5% (мотоциклдер); 31.8-32.9% (жолаушылар көліктері); 31.9-33.2% (жеңіл жүк көліктері); 31.9-33.3% (ауыр жүк көліктері). Берілген есептеулер эксперименттік зерттеулерде де, сандық модельдеуде де есептік жағдайларды модельдеуге қызығушылық тудырады. Алынған есептеу нәтижелері жол жағдайларын сандық немесе ірі көлемді модельдеуде есептеу схемаларын дәлірек жасауға мүмкіндік береді.*

Түйін сөздер: *цемент-бетон жабын, контактілік кернеулер, шиналық қысым, көлік жүктемелері, жол жүктемесін модельдеу, сандық модельдеу*

***Автор-корреспондент**
Ляйля Кабдырова, e-mail: leila_0781@mail.ru

https://doi.org/10.51488/1680-080X/2026.1-14
Алынды 04 ақпан 2026; Қайта қаралды 18 ақпан 2026; Қабылданды 05 наурыз 2026

УДК 691.537
МРНТИ 67.09.33
НАУЧНАЯ СТАТЬЯ

АНАЛИЗ НАПРЯЖЕНИЙ В ЦЕМЕНТОБЕТОННЫХ ПОКРЫТИЯХ ОТ ТРАНСПОРТНЫХ НАГРУЗОК

Л.Т. Кабдырова[1,*], Р.Е. Лукпанов[1], Ф.Б. Абдушкуров[2], М. Караджасу[3]

[1]Евразийский национальный университет имени Л.Н. Гумилева, 010000, Астана, Казахстан
[2]ТОО «Технобиус», 010000, Астана, Казахстан
[3]Эскишехирский технический университет, 26000, Эскишехир, Турция

Аннотация. *В статье представлены расчеты нормальных напряжений, возникающих под воздействием транспортных нагрузок от различных типов транспортных средств, для последующего моделирования истираемости пропиточных составов в цементобетонных дорожных покрытиях. Целью исследования была оценка нормальных напряжений, возникающих при ударе транспортных средств, с учетом изменчивости пятна контакта в результате снижения или повышения давления в шине. В работе проведена оценка уровней нормальных напряжений при воздействии транспортных нагрузок с учетом вариативности площади контакта шины с покрытием, обусловленной изменением давления в шинах. Транспортные средства, от велосипедов до тяжелых грузовых автомобилей, были классифицированы по категориям A1-A5 в порядке возрастания массы. Результаты представлены в виде диапазонов, где нижние границы соответствуют наиболее легким транспортным средствам в каждой категории при минимальном давлении в шинах, а верхние - наиболее тяжелым при максимальном давлении. Показано, что давление в шинах оказывает существенное влияние на напряженное состояние дорожного покрытия, увеличивая нормальные напряжения на 28.6-30.3% (велосипеды); 30.9-33.5% (мотоциклы); 31.8-32.9% (легковые автомобили); 31.9-33.2% (легкие грузовые автомобили); 31.9-33.3% (грузовые автомобили). Представленные расчеты представляют интерес при моделировании расчетных ситуаций как в экспериментальных исследованиях, так и при численном моделировании. Полученные результаты расчетов позволят более точно разработать схемы расчета при численном или крупномасштабном моделировании дорожных ситуаций.*

Ключевые слова: *цементобетонное покрытие, контактные напряжения, давление в шинах, транспортные нагрузки, моделирование дорожной нагрузки, численное моделирование*

***Автор-корреспондент**
Ляйля Кабдырова, e-mail: leila_0781@mail.ru

https://doi.org/10.51488/1680-080X/2026.1-14
Поступила 04 февраля 2026; Пересмотрено 18 февраля 2026; Принято 05 марта 2026

ACKNOWLEDGEMENTS/SOURCE OF FUNDING

This research was carried out within the grant funding of the Science Committee of the Ministry of Science and Higher Education of the Republic of Kazakhstan (Grant No. AP26197579 “Development of the composition and production technology of an anti-icing agent for concrete roads based on latex emulsion and agricultural waste”).

CONFLICT OF INTEREST

The authors state that there is no conflict of interest.

The authors declare that no generative artificial intelligence technologies or technologies based on artificial intelligence were used in the preparation of this article.

АЛҒЫС / ҚАРЖЫЛАНДЫРУ КӨЗІ

Зерттеу Қазақстан Республикасы Ғылым және жоғары білім министрлігі Ғылым комитетінің AP26197579 «Латекс эмульсиясы мен ауыл шаруашылығы қалдықтарына негізделген бетон жолдарға арналған мұзға қарсы агенттің құрамын және оны өндіру технологиясын әзірлеу» гранттық қаржыландыруы шеңберінде жүргізілді.

МҮДДЕЛЕР ҚАҚТЫҒЫСЫ

Авторлар мүдделер қақтығысы жоқ деп мәлімдейді.

Авторлар мақаланы дайындау кезінде генеративті жасанды интеллект технологиялары мен жасанды интеллектке негізделген технологиялар қолданылмағанын айтады..

БЛАГОДАРНОСТИ/ИСТОЧНИК ФИНАНСИРОВАНИЯ

Исследование выполнено в рамках грантового финансирования Комитета науки Министерства науки и высшего образования Республики Казахстан (грант № AP26197579 «Разработка состава и технологии производства противогололёдного реагента для бетонных дорог на основе латексной эмульсии и отходов сельского хозяйства»).

КОНФЛИКТ ИНТЕРЕСОВ

Авторы заявляют, что конфликта интересов нет.

Авторы заявляют о том, что при подготовке статьи не использовались технологии генеративного искусственного интеллекта и технологии, основанные на искусственном интеллекте

1 INTRODUCTION

Road construction plays a key role in the economic development of any country. In modern road construction practice, the emphasis is on creating safe and comfortable conditions for traffic, as well as ensuring the reliability and durability of the road surface. To achieve these goals, various technologies and construction methods are used, the choice of which depends on the type of road surface. The most commonly used materials for road surfaces are concrete and asphalt. Each has its own advantages and limitations **(Saleh et al., 2024).** Concrete roads have a number of significant advantages over asphalt concrete roads, including high wear resistance and long service life, which reduces the need for repairs. The use of concrete is also environmentally preferable, as it is made from natural components. The ability to withstand temperature changes and resist local deformation makes concrete pavements an ideal solution for heavy loads **(Ma et al., 2014)**. However, the main disadvantage is the higher cost compared to asphalt. The increased porosity of concrete can lead to ice formation at sub-zero temperatures, which impairs wheel traction and increases the risk of accidents.

The proposed method of combating icing is a technological process of applying a protective layer with ice-repellent properties to the surface of concrete roads. This layer, which is a solution of soluble polymers, penetrates into the concrete structure, and its effectiveness depends on the depth of this penetration. Given that concrete has the ability to absorb moisture, the optimal solution is to use a concentrated impregnation solution mixed with water. Water penetrates the pores of the concrete, carrying polymer components with it and creating a thin film around the pores that reduces the adhesion of ice to the surface. This allows the ice to break easily even with minor mechanical impact **(Pacheco-Torgal et al., 2013)**. Colloidal dispersed polymer and keratin obtained from agricultural waste are used as polymers, which ensures stability of supply and reduces production costs. The raw materials for the keratin-containing coating include animal wool, hair, horns, and hooves. This makes the development of an ice-repellent coating particularly relevant for the Republic of Kazakhstan, as it corresponds to the priority task of processing agricultural waste and creating new materials.

Thus, the research is aimed at substantiating the effectiveness of a polymer-based impregnation capable of reducing ice adhesion to cement concrete pavements while maintaining practical applicability and economic feasibility.

In the study by **(Persson et al., 1994)**, a technology for anti-icing coatings based on vulcanized rubber was proposed, utilizing sulfur, its compounds, or metal oxides. The elasticity of such materials prevents ice formation on road surfaces, particularly on porous asphalt pavements that facilitate rapid water drainage.

In international research **(Balordi et al., 2022)** demonstrated a simple and easily adaptable method for producing superhydrophobic and icephobic zinc coatings. Zinc oxide nanostructures are formed via a hydrothermal process at 90°C for less than 30 minutes, followed by treatment with stearic acid or fluoroalkylsilane, resulting in surfaces with static contact angles above 165° and sliding angles below 1°. These coatings retain their properties even after one month of exposure to harsh conditions, effectively reducing ice formation.

In the work **(Macelloni et al., 2000)** a method for ice prevention based on microwave radiometry (millimeter-wave range) was proposed. The approach relies on localized heating of the road surface using microwave radiation generators. However, its practical implementation is limited due to high costs and operational instability.

In scientific research **(Ma et al., 2014)** examines the treatment of the road surface layer with hydrophobic agents. The effectiveness was evaluated based on contact angle, shear strength, wear resistance, and skid resistance. The results showed that this method reduces the adhesion between ice and asphalt concrete, making it a promising solution for winter road maintenance.

Chemical compounds and salts capable of melting ice are widely used to prevent road icing. However, concrete pavements are sensitive to the aggressive environment formed when these substances interact with water **(Furmidge et al., 1962)**, which can lead to pavement deterioration and

vehicle corrosion **(Dan et al., 2014)**. Moreover, the continuous use of de-icing agents requires repeated application during each icing event. Due to variable weather conditions, this approach is not always efficient and can be costly **(Medeiros et al., 2008)**.

As an alternative, sand is used in some countries to improve tire traction on icy roads **(Zhan et al., 2014)**. However, this method provides only a short-term effect and requires frequent reapplication.

A promising solution to the icing problem is the use of penetrating treatments capable of reducing or partially preventing ice formation on concrete pavements.

The significance of this study lies in the development of an ice-repellent composition based on keratin-containing substances derived from the livestock industry and modified with water-soluble polymers. The proposed technology involves forming a protective film with ice-repellent properties on the surface of concrete roads. This polymer-containing solution penetrates the material structure, and its effectiveness depends on the depth of penetration. As a result, the porous structure of concrete is encapsulated, creating a stress gradient layer that prevents the bonding of ice to the concrete matrix, causing the ice to fracture even under minor mechanical impact.

2 MATERIALS AND METHODS

The impregnating composition of the anti-icing agent is represented by an aqueous solution of polymer components. Colloidal dispersed polymer and keratin will be used as polymer components. Keratin is an agricultural waste product, the regional availability of which can ensure its uninterrupted production. The keratin-containing raw materials required for the production of ice-repellent coatings are of animal origin and include animal wool, hair, horns, hooves, and others. **Figure 1** shows a diagram of the production of the impregnating composition. The crushed keratin-containing component is loaded into the cooking boiler with a weak concentration of boric acid in water (the ratio of water to raw material is 1:3 by weight). At the same time, a mixture of urea in water is added (the water ratio is 2:3 by weight to raw material). After the hydrolysis process at a temperature of 130°C for up to 10 hours, a pH acidity neutralizer, represented by iron sulfate, is added to the cooled mass.

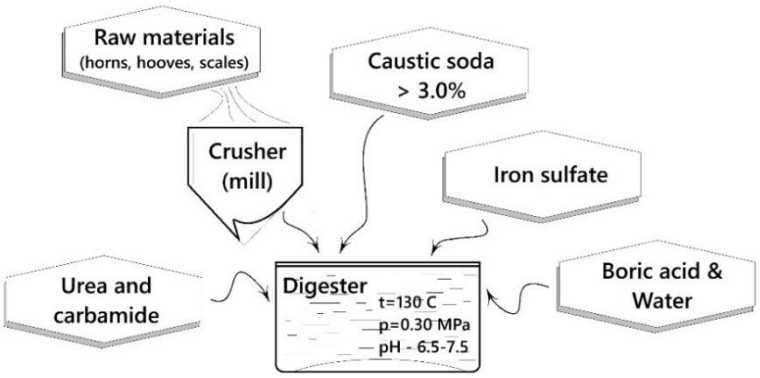

Figure 1 - Diagram of the impregnation composition production process (author's material)

The study also evaluated normal stresses on road surfaces under vehicle loads (ranging from bicycles to trucks, categories A1-A5), taking into account variations in tire pressure and contact area. Using linear graphical methods of tire characteristics, stress ranges were obtained that can serve as a basis for accurate numerical and large-scale modeling of road loading conditions.

To simulate stresses in scale models, motor vehicles were divided into five categories based on their load capacity:

- A1 - bicycles;

- A2 - motorcycles (mopeds);
- A3 - passenger cars;
- A4 - light trucks and buses with very low capacity;
- A5 - trucks and buses.

The characteristics of each category of motor vehicle for calculating stresses are presented in **Tables 1-5**.

Table 1
Specifications for pneumatic bicycle tires **(GOST 4750)**

Tire designation according to GOST	Layer norm	Outer diameter of tires, m	Tire profile width, m	Static tire radius, m	Maximum permissible load, t
Minimum values for linear load					
56-205	1	0.323	0.059	0.0143	0.2943
Maximum linear load values					
28-622	1	0.678	0.028	0.0081	0.5886

Table 2
Specifications for pneumatic tires for motorcycles (mopeds) **(GOST 4754)**

Tire designation according to GOST	Layer norm	Outer diameter of tires, m	Tire profile width, m	Static tire radius, m	Maximum permissible load, t
Minimum values for linear load					
2.25-19	4	0.61	0.062	0.29	0.98
Maximum linear load values					
4.00-10C	4	0.46	0.108	0.213	3.19

Table 3
Specifications for pneumatic tires for passenger cars **(GOST 52900)**

Tire designation according to GOST	Layer norm	Outer diameter of tires, m	Tire profile width, m	Static tire radius, m	Maximum permissible load, t
Minimum values for linear load					
135/80 R12	1	0.521	0.14	0.239	2.599
Maximum linear load values					
185-14/7.35-14	1	0.668	0.185	0.31	5.492

Table 4
Specifications for pneumatic tires for light trucks and small buses **(GOST 4754)**

Tire designation according to GOST	Layer norm	Outer diameter of tires, m	Tire profile width, m	Static tire radius, m	Maximum permissible load, t
Minimum values for linear load					
5.90-13C	1	0.62	0.154	0.292	4.168
Maximum linear load values					
225/75R16C	1	0.744	0.228	0.338	14.22

Table 5
Specifications for pneumatic tires for trucks and buses **(GOST 5513)**

Tire designation according to GOST	Layer norm	Outer diameter of tires, m	Tire profile width, m	Static tire radius, m	Maximum permissible load, t
Minimum values for linear load					
8.25R20	10	0.962	0.234	0.453	16.190
Maximum linear load values					
15R22.5	18	1.072	0.389	0.505	44.150

Obviously, the normal stress transmitted by the wheel depends not only on the load capacity, but also on the number of axles, wheels, and wheel pressure. The latter characterizes the contact patch or the wheel's bearing area.

In this study, the dimensions and contact area of the pneumatic tire footprint were determined using the mathematical model proposed by V. L. Biderman, which is based on the parameters of the tire universal characteristic (UCT) **(Lipkan et al., 2019)**. Since this approach employs the ply rating index as a parameter characterizing the tire's stiffness properties, it is assumed that an increase in the ply rating corresponds to an increase in tire stiffness, which is taken into account when calculating the contact patch area. The model represents the deformed tire as a toroidal shell interacting with a rigid flat surface. The footprint contour is approximated by an ellipse, consistent with a widely adopted engineering assumption.

The contour area of the tire contact patch is determined using the ellipse area formula:

$$F_{k_i} = \frac{\pi}{4} a_{k_i} b_{k_i} \quad (1)$$

where a_{k_i} - the contact patch length in the longitudinal direction, m;

b_{k_i} - the contact patch width in the transverse direction, m.

The dimensions of the tire tread contact patch using universal tire characteristics parameters are proposed to be calculated using the following formulas:

$$a_{k_i} = c_3 \sqrt{D} \cdot f_{ш_i} - f_{шi}^2 \quad (2)$$

$$b_{k_i} = 2\sqrt{2R_{пр}} \cdot f_{ш_i} - f_{шi}^2 \quad (3)$$

where D - is the outer diameter of the tire, m;

$f_{ш_i}$ - vertical tire deflection (settlement), m;

$R_{пр}$ - specified tire profile radius, m;

c_3 - empirical contact patch shape coefficient.

The equivalent profile radius is determined by the following expression:

$$R_{пр} = (B + H)/2.5 \quad (4)$$

where B - tire profile width, m;

H=(D-d)/2 - tire profile height, m;

d - nominal rim diameter, m.

$$c_3 = \frac{20.5}{11.9 + \left|\frac{D}{B} - \frac{|n-9|}{2} - 3\right|} \quad (5)$$

where n - tire aspect ratio index.

The value $[f_ш]$ can be roughly determined using the following formula:

$$[f_ш] \approx D/2 - r_{ст} \quad (6)$$

where $r_{ст}$ - is the static radius, m.

Thus, the Biderman model makes it possible to determine the geometric parameters of the contact patch using measurable tire geometry and its vertical deflection. It should be noted that the model is semi-empirical and is applicable for estimating the contour area of the tire contact patch on a rigid flat surface without considering the distribution of contact stresses.

At the same time, the approach does not account for the actual stress distribution within the contact patch, the influence of dynamic factors (vehicle speed and surface micro-roughness), foundation deformability, or potential variations in tire properties under different temperature and operating conditions. Therefore, the obtained values should be treated as calculated ranges of normal stresses intended for engineering assessment and for use in pavement loading simulations.

4 RESULTS AND DISCUSSION

Figures 2-4 show the ranges of tire technical characteristics by vehicle category required for calculating normal contact patch pressure.

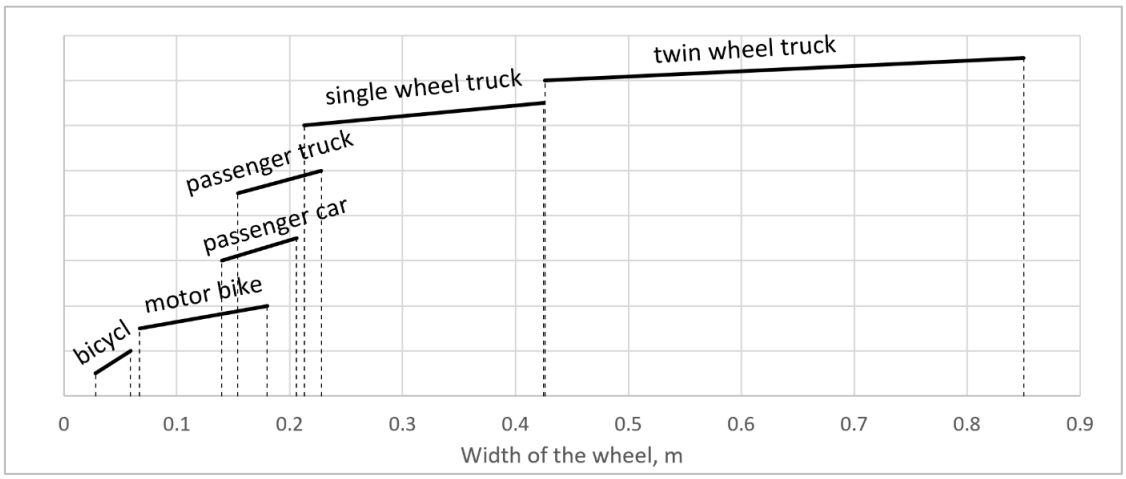

Figure 2 - Range of tire widths by category (author's material)

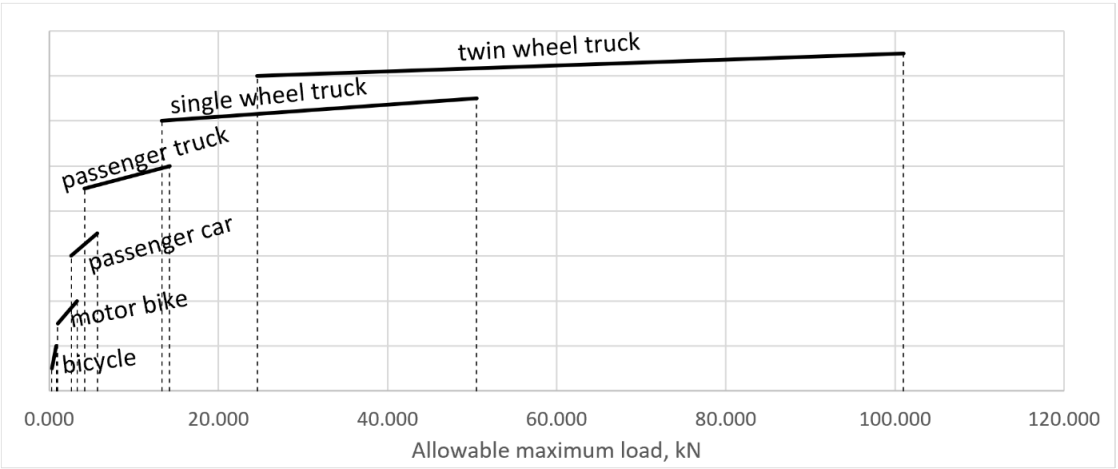

Figure 3 - Range of permissible loads on tires by category (author's material)

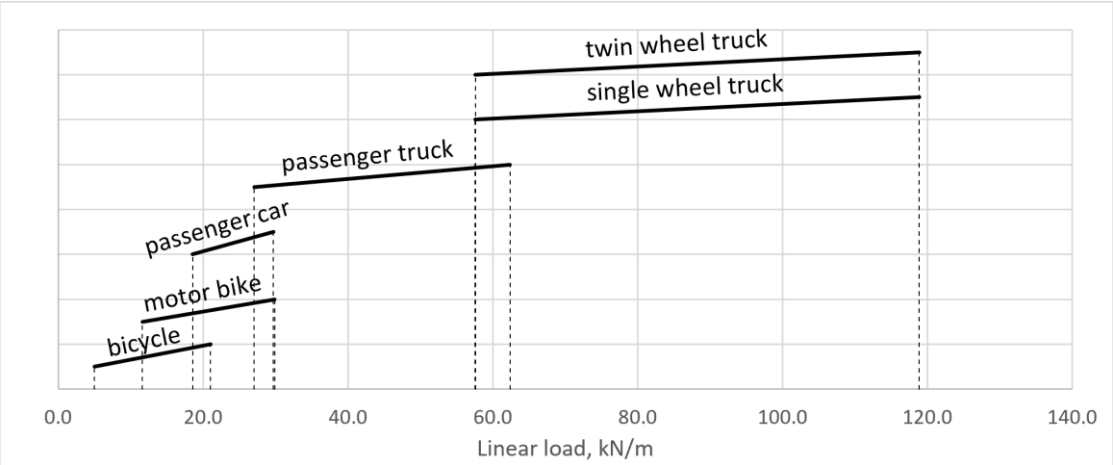

Figure 4 - Range of linear loads on tires by category (author's material)

Tables 6-10 present calculations of stresses transmitted from motor vehicles to the road depending on the wheel contact patch. The latter was determined from the standard (ρ_{St}), minimum (ρ_{min}) and maximum (ρ_{max}) tire pressures. According to the requirements, the deviation of pressure from the standard value is within ±2-5%, but in the calculations, a larger value of ±15% was taken, which will significantly increase the stress range and will not contradict the real operating conditions of vehicles. When the pressure decreases, the static radius will decrease and the static deflection will increase, therefore the contact patch will increase. Conversely, when the pressure increases, the contact patch will increase, and consequently, the stress transmitted by the wheel will also increase. The values of the maximum permissible loads, static radii, tire widths, outer diameters, and rim diameters were taken from GOST.

Table 6
Results of bicycle stress calculations

Tire type	Spot area (S_t), cm^2			Stress on the road (σ_t)					
				ρ_{min}		ρ_{St}		ρ_{max}	
	ρ_{min}	ρ_{St}	ρ_{max}	kN/m^2	kg/cm^2	kN/m^2	kg/cm^2	kN/m^2	kg/cm^2
56-205	46.5	53.6	60.5	48.7	0.65	54.9	0.56	63.4	0.50
40-406	44.1	50.9	57.3	111.3	1.47	125.3	1.28	144.4	1.14
30-445	33.9	39.0	43.8	89.7	1.18	100.6	1.03	115.6	0.91
47-507	45.3	52.3	58.9	133.2	1.77	150.1	1.53	173.1	1.36
37-533	37.3	43.0	48.3	132.0	1.74	148.4	1.51	170.9	1.35
37-540	35.3	40.6	45.7	150.4	1.98	169.1	1.72	194.6	1.53
40-559	39.7	45.8	51.5	114.2	1.51	128.5	1.31	148.1	1.16
48-559	47.2	54.5	61.5	119.6	1.59	134.9	1.38	155.8	1.22
32-590	29.8	34.2	38.4	153.3	2.02	172.0	1.75	197.7	1.56
32-622	31.2	35.9	40.3	170.3	2.24	191.2	1.95	219.9	1.74
37-622	36.0	41.5	46.6	147.3	1.95	165.6	1.69	190.8	1.50
40-622	40.7	47.0	52.9	139.0	1.84	156.6	1.60	180.6	1.42
32-630	29.3	33.7	37.8	168.8	2.22	189.4	1.93	217.7	1.72
47-406	47.0	54.2	61.0	104.4	1.38	117.7	1.20	135.7	1.07
47-622	43.6	50.3	56.7	129.7	1.72	146.2	1.49	168.7	1.32
47-305	48.5	56.0	63.0	77.9	1.03	87.7	0.89	101.0	0.79
47-559	44.5	51.3	57.9	144.1	1.91	162.4	1.66	187.4	1.47
28-622	25.6	29.4	32.9	178.7	2.34	200.2	2.04	229.8	1.82

Table 7
Results of motorcycle stress calculations

Tire type	Spot area (S_t), cm^2			Stress on the road (σ_t)					
				ρ_{min}		ρ_{St}		ρ_{max}	
	ρ_{min}	ρ_{St}	ρ_{max}	kN/m^2	kg/cm^2	kN/m^2	kg/cm^2	kN/m^2	kg/cm^2
For motorcycles without sidecars									
6.70 -10	94.4	110.3	125.8	174.7	1.78	199.3	2.03	232.7	2.37
3.25-16	106.5	123.8	140.6	139.5	1.42	158.5	1.62	184.2	1.88
3.50-16	102.7	119.5	135.8	166.1	1.69	188.8	1.93	219.6	2.24
3.00-18	78.2	91.1	103.8	189.0	1.93	215.3	2.20	250.8	2.56
3.50-18	97.4	113.6	129.3	169.9	1.73	193.5	1.97	225.5	2.30
3.50/85-18	63.9	74.7	85.3	143.8	1.47	164.2	1.67	191.8	1.96
4.00/85-18	72.5	84.7	96.7	233.3	2.38	266.5	2.72	311.4	3.18
2.50-19	76.2	88.6	100.7	155.9	1.59	177.1	1.81	205.9	2.10
3.00-19	85.2	99.1	112.7	111.4	1.14	126.7	1.29	147.4	1.50
3.25-19	114.2	132.5	150.2	142.3	1.45	161.4	1.65	187.3	1.91
3.25-19*	74.1	86.5	98.7	210.8	2.15	240.4	2.45	280.5	2.86
For motorcycles with sidecars									
3.50-18	103.4	120.5	137.3	194.3	1.98	221.4	2.26	258.1	2.63
3.75-18	103.6	120.6	137.3	194.4	1.98	221.2	2.26	257.6	2.63
3.25-19	114.2	132.5	150.2	167.8	1.71	190.3	1.94	220.8	2.25
3.75-19	128.6	149.4	169.6	177.6	1.81	201.6	2.06	234.1	2.39
4.00-19	161.7	187.1	211.7	155.3	1.58	175.6	1.79	203.3	2.07
For motorized wheelchairs, motor scooters, and mopeds									
3.00-10	43.4	50.8	58.0	184.4	1.88	210.6	2.15	246.1	2.51
4.00-10	90.5	105.3	119.7	193.3	1.97	219.9	2.24	255.8	2.61
4.00-10C	92.1	107.1	121.8	261.8	2.67	297.6	3.04	346.2	3.53
5.00-10	74.5	87.1	99.4	197.3	2.01	225.3	2.30	263.2	2.68
2.50/85-16	55.4	64.6	73.6	181.3	1.85	206.6	2.11	240.8	2.46
2.25-19	66.8	77.6	88.2	111.2	1.13	126.4	1.29	146.9	1.50

Table 8
Results of stress calculations for passenger cars

Tire type	Spot area (S_t), cm^2			Stress on the road (σ_t)					
				ρ_{min}		ρ_{St}		ρ_{max}	
	ρ_{min}	ρ_{St}	ρ_{max}	kN/m^2	kg/cm^2	kN/m^2	kg/cm^2	kN/m^2	kg/cm^2
135/80R12	116.6	135.5	154.0	168.8	1.72	191.7	1.96	222.8	2.27
155/80R13	156.9	182.1	206.6	175.6	1.79	199.3	2.03	231.4	2.36
165/80R13	169.9	197.3	223.9	179.6	1.83	203.8	2.08	236.7	2.41
175/80R13	180.7	209.9	238.2	185.3	1.89	210.3	2.14	244.2	2.49
165/80R14	175.9	204.4	232.0	183.8	1.87	208.7	2.13	242.5	2.47
175/80R16	198.9	231.1	262.4	187.7	1.91	213.1	2.17	247.6	2.53
155/70R13	125.2	145.5	165.4	189.7	1.93	215.6	2.20	250.7	2.56
165/70R13	143.1	166.3	189.0	186.8	1.91	212.2	2.16	246.7	2.52
175/70R13	153.5	178.4	202.7	196	2.00	222.6	2.27	258.8	2.64
185/70R13	172.6	200.6	227.8	178.7	1.82	202.9	2.07	235.8	2.40
175/70R14	138.9	161.7	184.0	226.5	2.31	257.7	2.63	300.1	3.06
185/70R14	178.0	206.9	235.0	198.2	2.02	225.1	2.30	261.7	2.67
205/70R14	216.1	251.0	284.9	199.6	2.04	226.6	2.31	263.2	2.68
185/65R13	145.5	169.3	192.5	201.8	2.06	229.4	2.34	266.8	2.72
155-13/6.15-13	141.1	164.2	186.9	194.2	1.98	221	2.25	257.2	2.62
165-13/6.45-13	132.1	154.0	175.5	206.8	2.11	235.7	2.40	274.7	2.80
175-13/6.95-13	151.4	176.3	200.6	202.9	2.07	230.9	2.35	268.8	2.74
185-14/7.35-14	173.7	202.3	230.3	238.5	2.43	271.5	2.77	316.2	3.22
175/80-16	146.6	171.0	194.9	213.8	2.18	243.8	2.49	284.3	2.90

Table 9
Results of stress calculations for light trucks

Tire type	Spot area (S_t), cm^2			Stress on the road (σ_t)					
				ρ_{min}		ρ_{St}		ρ_{max}	
	ρ_{min}	ρ_{St}	ρ_{max}	kN/m^2	kg/cm^2	kN/m^2	kg/cm^2	kN/m^2	kg/cm^2
Radial tires									
185/80R15C	192.5	223.9	254.5	337.2	3.44	383.3	3.91	445.8	4.55
215/80R16C	185.7	216.7	247.2	410.6	4.19	468.4	4.78	546.6	5.57
225/75R16C	270.2	313.9	356.5	398.9	4.07	453.0	4.62	526.3	5.37
Diagonal tires									
5.90-13C	121.8	142.1	162.1	257.2	2.62	293.3	2.99	342.2	3.49
6.40-13C	138.7	161.8	184.6	265.6	2.71	302.9	3.09	353.5	3.60
215/90-15C	212.3	247.7	282.4	269.1	2.74	306.9	3.13	358.0	3.65
6.50-16C	166.5	194.4	221.8	287.4	2.93	327.9	3.34	382.9	3.90
175/80-16C	146.6	171.0	194.9	259.0	2.64	295.3	3.01	344.5	3.51

Table 10
Results of stress calculations for trucks

	Spot area (S_t), cm^2			Stress on the road (σ_t)					
				ρ_{min}		ρ_{St}		ρ_{max}	
	ρ_{min}	ρ_{St}	ρ_{max}	kN/m^2	kg/cm^2	kN/m^2	kg/cm^2	kN/m^2	kg/cm^2
Diagonal tires									
7.50-20	243.3	284.3	324.7	410.8	4.19	469.3	4.79	548.4	5.59
7.50-20	243.3	284.3	324.7	468.4	4.78	535.0	5.46	625.3	6.38
7.50-20	257.7	301.1	344.0	513.4	5.24	586.5	5.98	685.4	6.99
8.25-20	290.3	339.2	387.5	417.8	4.26	477.3	4.87	557.7	5.69
8.25-20	297.2	347.3	396.7	469.9	4.79	536.8	5.47	627.2	6.40
8.25-20	274.8	321.1	366.7	551.1	5.62	629.5	6.42	735.6	7.50
9.00-20	339.4	396.6	453.0	485.0	4.95	553.9	5.65	647.3	6.60
9.00-20	314.2	367.1	419.3	587.9	5.99	671.4	6.85	784.6	8.00
10.00-20	382.7	447.2	510.7	453.3	4.62	517.7	5.28	604.8	6.17
10.00-20	354.6	414.3	473.1	549.6	5.60	627.6	6.40	733.3	7.48
10.00-20	330.2	385.9	440.7	667.9	6.81	762.7	7.78	891.1	9.09
11.00-20	393.6	459.8	525.0	560.6	5.72	640.1	6.53	747.8	7.63
11.00-20	366.8	428.5	489.2	651.6	6.64	744.1	7.59	869.2	8.86
12.00-20	439.4	513.2	586.0	502.2	5.12	573.4	5.85	669.8	6.83
12.00-20	409.7	478.6	546.4	601.4	6.13	686.6	7.00	802.1	8.18
12.00-20	383.8	448.3	511.9	718.8	7.33	820.7	8.37	958.6	9.78
12.00-24	446.8	521.7	595.3	659.2	6.72	752.2	7.67	878.2	8.96
Radial chamber tires									
7.50R20	276.5	322.8	368.4	362.1	3.69	413.2	4.21	482.5	4.92
7.50R20	276.5	322.8	368.4	412.9	4.21	471.2	4.80	550.1	5.61
7.50R20	292.9	341.9	390.2	452.6	4.62	516.5	5.27	603.0	6.15
8.25R15	299.5	348.7	396.8	673.7	6.87	766.6	7.82	892.6	9.10
8.25R20	348.3	406.4	463.4	349.4	3.56	398.4	4.06	464.8	4.74
8.25R20	354.6	413.7	471.8	395.1	4.03	450.5	4.59	525.6	5.36
8.25R20	327.5	382.2	436.0	463.6	4.73	528.8	5.39	617.1	6.29
9.00R20	458.9	534.9	609.4	360.5	3.68	410.7	4.19	478.7	4.88
9.00R20	424.5	494.9	563.9	435.0	4.44	495.7	5.05	577.9	5.89
10.00R20	455.5	531.0	605.1	429.7	4.38	489.6	4.99	570.9	5.82
10.00R20	424.2	494.6	563.6	522.2	5.33	595.1	6.07	693.8	7.07
11.00R20	485.0	565.6	644.6	456.6	4.66	520.4	5.31	606.8	6.19
11.00R20	452.0	527.0	600.7	547.0	5.58	623.5	6.36	727.0	7.41
12.00R20	494.6	577.2	658.4	447.0	4.56	509.9	5.20	595.0	6.07
12.00R20	461.2	538.2	613.9	535.3	5.46	610.6	6.23	712.5	7.27
12.00R20	432.0	504.1	575.0	639.8	6.52	729.8	7.44	851.6	8.68
12/80R20	371.5	433.5	494.4	644.8	6.58	735.5	7.50	858.2	8.75
Radial chamber tires									
370/70R20	403.6	470.8	536.8	758.2	7.73	864.5	8.82	1008.4	10.28
12.00R24	562.2	655.0	745.9	526.1	5.36	599.0	6.11	697.9	7.12

Table 10 (continued). Results of stress calculations for trucks

Radial tubeless tires									
10R22.5	358.0	417.0	474.8	516.6	5.27	588.2	6.00	685.2	6.99
11R22.5	394.1	459.1	522.8	562.9	5.74	641.0	6.54	746.8	7.62
11R22.5	394.1	459.1	522.8	591.0	6.03	673.0	6.86	784.1	8.00
12R22.5	433.8	505.5	575.6	553.8	5.65	630.7	6.43	734.8	7.49
12R22.5	433.8	505.5	575.6	570.8	5.82	650.1	6.63	757.4	7.72
15R22.5	362.9	423.9	484.1	912.1	9.30	1041.5	10.62	1216.7	12.41
275/80R22.5	375.4	437.1	497.5	621.0	6.33	706.9	7.21	823.2	8.39
295/80R22.5	351.3	409.8	467.3	703.1	7.17	801.8	8.18	935.4	9.54
295/80R22.5	351.3	409.8	467.3	745.3	7.60	849.9	8.67	991.5	10.11
315/80R22.5	431.0	502.3	572.0	642.3	6.55	731.5	7.46	852.4	8.69
350/80R22.5	424.4	495.4	565.1	746.4	7.61	851.5	8.68	993.8	10.13
11/70R22.5	333.5	388.4	442.1	665.7	6.79	757.8	7.73	882.6	9.00
315/70R22.5	420.3	489.2	556.4	572.9	5.84	651.7	6.65	758.5	7.73
315/70R22.5	420.3	489.2	556.4	626.0	6.38	712.0	7.26	828.7	8.45
425/65R22.5	446.8	521.6	595.3	848.7	8.65	968.5	9.88	1130.8	11.53

It can be observed that when tire pressure is low, the contact patch increases, thereby reducing road stress. For bicycles, the minimum road pressure at the minimum permissible tire pressure is 0.50 kg/cm² (48.7 kN/m²), and the maximum pressure at the maximum permissible tire pressure is 2.34 kg/cm² (229.8 kN/m²). The same values, under similar conditions, for motorcycles are: minimum stress - 1.13 kg/cm² (111.2 kN/m²); maximum stress - 3.53 kg/cm² (346.2 kN/m²). For passenger cars, the minimum stress is 1.72 kg/cm² (168.8 kN/m²) and the maximum stress is 3.22 kg/cm² (316.2 kN/m²). For light commercial vehicles, the minimum stress is 2.62 kg/cm² (257.2 kN/m²) and the maximum stress is 5.57 kg/cm² (546.6 kN/m²). For trucks, the minimum stress is 3.56 kg/cm² (349.4 kN/m²) and the maximum is 12.41 kg/cm² (1216.7 kN/m²). Thus, the results show that freight vehicles, due to their heavy weight relative to the size of their tires, exert the greatest stress on the road. Moreover, given the degree of freedom of large trucks relative to the width of the lane, the degree of abrasion of the tread increases significantly. That is, the width of the wheel's contact patch is smaller for large trucks than for small ones. Therefore, despite the relatively greater stress from a motorcycle (3.53 kg/cm² or 346.2 kN/m²) compared to a passenger car (3.22 kg/cm² or 316.2 kN/m²), the impregnating compound will be subject to greater wear due to abrasion caused by passenger vehicles.

For a clear comparative analysis of contact stress ranges generated by different vehicle categories, a graphical interpretation was performed **(Figure 5)**. The graph presents the minimum and maximum values of normal stresses transmitted to the pavement, allowing a visual comparison of the loading intensity associated with various vehicle types.

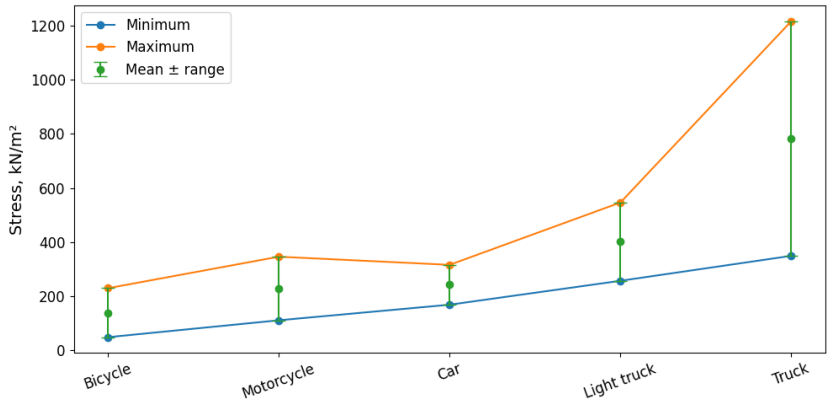

Figure 5 – Stress range diagram (author's material)

The analysis of the graphical relationship indicates a consistent increase in minimum contact stresses with growing vehicle mass, reflecting higher wheel loads under comparable contact patch

dimensions. For heavy vehicles, a substantial widening of the stress range is observed, which is associated with significant variability in operational parameters such as axle load, tire inflation pressure, and tire design characteristics.

It is also found that the maximum contact stresses of motorcycles and passenger cars are of similar magnitude despite differences in contact patch geometry. This can be explained by the smaller tire width of motorcycles and the resulting higher load localization. Overall, the graphical relationship demonstrates the dominant impact of heavy vehicles on pavement structures, manifested by a pronounced increase in maximum contact stresses and the formation of the most unfavorable loading conditions for pavement performance.

5 CONCLUSIONS

1. The article presents the results of studies of normal stresses transmitted by motor vehicles to the road for subsequent modeling of design situations in large-scale experiments or numerical modeling.

2. For each category of motor vehicles, calculations of normal stresses on the road surface have been performed: for category A1, the stress range is from 48.7 kN/m^2 (0.50 kg/cm^2) to 229.8 kN/m^2 (2.34 kg/cm^2); for A2, from 111.4 kN/m^2 (1.13 kg/cm^2) to 346.2 kN/m^2 (3.53 kg/cm^2); for A3, from 168.8 kN/m^2 (1.72 kg/cm^2) to 316.2 kN/m^2 (3.22 kg/cm^2); for A4 from 259.0 kN/m^2 (2.62 kg/cm^2) to 546.6 kN/m^2 (5.57 kg/cm^2); for A5 from 349.4 kN/m^2 (3.56 kg/cm^2) to 1216.7 kN/m^2 (12.41 kg/cm^2).

3. It was established that as the vehicle mass increases, the level of contact stresses and their range also increase. Heavy trucks produce the greatest impact on the pavement, generating the highest stress values and the most unfavorable loading conditions for the road structure.

4. The results obtained on the range of normal contact stresses for various categories of vehicles can be used as input parameters for modeling scenarios of road surface loading using numerical and physical modeling methods. The results of these studies will allow for modeling design scenarios that consider maximum stress (at the maximum tire pressure of vehicles with the highest load capacity in their category) and minimum stress (at the minimum tire pressure of vehicles with the lowest load capacity in their category). This will enable the determination of the maximum and minimum service life of the impregnating compound, taking into account the operational intensity of each specific type of vehicle.

REFERENCES

1. **Saleh M., Ahmed N., Moghaddam T. B., & Hashemian L.** (2024). Towards a high-performance asphalt concrete for extreme climatic conditions using asphaltenes and polyethylene terephthalate fibres. Construction and Building Materials. 420, 135573. https://www.sciencedirect.com/science/article/abs/pii/S0950061824007141
2. **Ma H., Yang R.,** & **Qian S. (**2014). Research on asphalt concrete pavement deicing technology. Journal of Southeast University (English Edition). 30(3), 336-342. https://doi.org/10.3969/j.issn.1003-7985.2014.03.015
3. **Pacheco-Torgal F., & Labrincha J. A.** (2013). Biotech cementitious materials: Some aspects of an innovative approach for concrete with enhanced durability. Construction and Building Materials. 40, 1136-1141. https://doi.org/10.1016/j.conbuildmat.2012.09.080
4. **Andersson L.-O. & Persson S.** (1994). Ice adhesion to rubber materials. Journal of Adhesion Science and Technology. 8(2), 117-132. WO1992008767A1.
5. **Balordi M., Cammi A., Casali A., Pini F., & Santucci de Magistris G.** (2025). On the Hydrophobicity, Superhydrophobicity and Icephobicity of Etched Aluminum Surfaces. Coatings. 15(11), 1328. https://doi.org/10.3390/coatings15111328

6. **Macelloni G., Ruisi R., Pampaloni P., & Paloscia S.** (1999). Detection of ice sheet on asphalt roads. Microwave Radiometry and Remote Sensing of the Earth's Surface and Atmosphere. 891-893. IEEE. https://doi.org/10.1109/IGARSS.1999.774476
7. **Furmidge C. G. L.** (1962). Studies at phase interfaces. I: The sliding of liquid drops on solid surfaces and a theory for spray retention. Journal of Colloid Science. 17(4), 309-324. https://doi.org/10.1016/0095-8522(62)90011-9
8. **Dan H., Li L., Mei S., Liu Y., & Bai S.** (2014). Review of freezing mechanism of ice on pavement and skid resistance performance of pavement in moist mountain area. Journal of Wuhan University of Technology (Transportation Science and Engineering). 38(4), 719-724. https://doi.org/10.3963/j.issn.2095-3844.2014.04.004
9. **Medeiros M., & Helene P.** (2008). Efficacy of surface hydrophobic agents in reducing water and chloride ion penetration in concrete. Materials and Structures. 41(1), 59-71. https://doi.org/10.1617/s11527-006-9218-5
10. **Zhan H., Wittmann F. H., & Zhao T.** (2014). Chloride barrier for concrete in saline environment established by water repellent treatment. Restoration of Buildings and Monuments. 9(5), 535-550. https://doi.org/10.1515/rbm-2003-5792
11. **Lipkan A. V., Panasyuk A. N., & Kashbulgayanov R. A.** (2019). Justification for the choice of method for determining the parameters of the contact patch of a pneumatic wheeled vehicle with the supporting base [Obosnovanie vybora metoda opredeleniya parametrov kontaktnogo pyatna pnevmaticheskogo kolesnogo transportnogo sredstva s opornym osnovaniem] Bulletin of Science and Practice, 5(6), 212-228. https://doi.org/10.33619/2414-2948/43/27 (In Rus.).
12. **Aubakirova T.A., Myrzakasymova Zh.Zh., Pentaev T.P., Zhanakova R.K**. (2024). Control of engineering geodetic works during the reconstruction of the territory of the highway. Bulletin of the Kazakh Leading Academy of Architecture and Civil Engineering, 2 (92), 7-21. [Avtokölik jolynyñ aumağyn qayta qūru kezindegi injenerlik geodeziyalyq jūmystardy baqylau] https://doi.org/10.51488/1680-080X/2024.2-01 (In Kaz.).
13. **Apshikur B., Imankulova A.S., Kunanbayev A.K., Alimkulov M.M., Lesov K.** (2025). Development of an effective method for strengthening weak foundations of railway embankments. Bulletin of the Kazakh Leading Academy of Architecture and Civil Engineering, 4 (98), 108-128. https://doi.org/10.51488/1680-080x/2025.4-07
14. **Hall C.** (1977). Water movement in porous building materials-I: Unsaturated flow theory and its applications. Building and Environment, 12(2), 117-125. https://doi.org/10.1016/0360-1323(77)90040-3
15. **Akmalaiuly K., Koshkombayeva G.** (2024) Corrosion resistance of concrete in aggressive medi. Bulletin of the Kazakh Leading Academy of Architecture and Civil Engineering, 4 (94), 145-154. https://doi.org/10.51488/1680-080X/2024.4-11
16. **Kopzhasarov B.T., Akhmetov D.A., Zhagifarov A.M., Abdraimov I.E., Kuttybai M.T., Zhumadilova Zh.O.** (2024). Quality improvement effectiveness of road slabs produced using microsilica and fiber. Bulletin of the Kazakh Leading Academy of Architecture and Civil Engineering, 2(92), 76-90. [Kremniyalyq talshyqtardy paydalany arqylý jol taqtaişalarynyń sapasyn arttyru tiimdiligi] https://doi.org/10.51488/1680-080X/2024.2-06 (In Kaz.).
17. **Zhilkibayeva A.M.** (2024). Construction and operational properties of concrete on modified binder. Bulletin of the Kazakh Leading Academy of Architecture and Civil Engineering, 2 (92), 36-49. [Stroitel′no-eksploatatsionnye svoystva betonov na modifitsirovannom vyazhushchem] https://doi.org/10.51488/1680-080X/2024.2-03 (In Russ.).
18. **Lukpanov R. E., Dyussembinov D. S., Yenkebayev S. B., & Tsygulyov D. V.** (2021). Impregnation composition to increase the ice-phobic properties of concrete roads. In Digital technologies in construction engineering: Selected papers. Springer International Publishing, 305-311. https://doi.org/10.1007/978-3-030-81289-8_39